Mat. Res. Soc. Symp. Proc. Vol. 686 © 2002 Materials Research Society

Phase Transformations Induced by Arsenic Implants into Silicon

James P. Lavine[1], David D. Tuschel[2], and Donald L. Black[2]

[1]Digital and Applied Imaging, Image Sensor Solutions, Eastman Kodak Company, Rochester, NY 14650-2008, U.S.A.
[2]Imaging Materials & Media, R & D, Analytical Technology Division, Eastman Kodak Company, Rochester, NY 14650-2132, U. S. A.

ABSTRACT

Micro-Raman spectroscopic investigations of arsenic-implanted silicon show lines characteristic of silicon crystallites even at implant doses above the amorphization threshold. The intensity and frequency of occurrence of the lines increase with the implanted dose. Polarization/orientation Raman studies indicate the crystallites are silicon in the hexagonal phase (Si-IV) and silicon in the diamond phase (Si-I). The latter are oriented differently than the substrate silicon. Monte Carlo simulations of the arsenic ion energy loss and published molecular dynamics studies suggest that each arsenic ion deposits sufficient energy to locally melt the silicon lattice. This is taken as the basis of the present attempt to explain the origin of the crystallites. A one-dimensional numerical model is developed to determine the time scale for the liquid silicon to solidify. The effect of amorphous silicon on the solidification is also investigated.

INTRODUCTION

As part of a study of ion-implanted silicon, Raman spectroscopy was applied to a series of arsenic-implanted silicon samples [1]. The dose varied from 2×10^{13} to 5×10^{15} As/cm^2. Macro-Raman spectroscopy showed the expected amorphous silicon broad band, which strengthened as the dose increased. This was accompanied by the decrease and eventual disappearance of the substrate optical phonon line at 520 cm^{-1}, when the arsenic dose exceeded 5×10^{14} As/cm^2. However, micro-Raman spectroscopy revealed narrow lines at ~508 cm^{-1} and 520 cm^{-1}, even for the 5×10^{15} As/cm^2 samples. Additional experimental work appeared to tie the narrow lines to specific locations with observable surface features [2,3]. We became aware that additional phases of silicon exist [4] and that there is a hexagonal phase, Si-IV, with a Raman line at 508 cm^{-1} [5]. Si-IV had been observed in arsenic-implanted silicon by Tan et al. [6] and in deposited polycrystalline silicon [7]. Tan et al. proposed a transformation from the diamond phase of silicon to Si-IV with the required energy coming from the implanted arsenic as it slowed down in the silicon.

In this work, we present Raman spectroscopy results that clarify our earlier observations and further elucidate the phases of silicon present. The second section contains a brief account of the experiments and new data. The third section considers the state of the silicon during the implant. It has a numerical model that simulates the cooling of the implanted silicon region and its phase

transformation from liquid to crystalline silicon. The fourth section describes the effects of increased arsenic implant dose and the appearance of amorphous silicon. The final section has the conclusions, some speculations, and an indication of future work.

EXPERIMENTAL METHODS AND RESULTS

Two series of 150 keV arsenic implants were done through 0.06 μm of thermally-grown silicon dioxide into silicon. The dose ranged from 2×10^{13} to 5×10^{15} As/cm^2 and the flux was of the order of 1.4×10^{13} As/cm^2-s. The beam current ranged from 180 to 763 microamperes and increased with the dose for the second series of implants. In addition, device wafers with 150 keV arsenic implants at a dose of 2×10^{15} As/cm^2 were pulled after the implant and after an anneal at 1000° C. The micro-Raman spectroscopy was done in the backscattering configuration with an Instruments SA S3000 spectrometer. The excitation wavelength was 514.5 nm and the incident power was 5 mW or less. Polarization/ Orientation (P/O) spectra were also captured with this instrument. Transmission electron microscopy (TEM) was done to show the 5×10^{15} As/cm^2 implant produced about a 0.11 μm-thick surface layer of amorphous silicon. The amorphous silicon/crystalline silicon interface was found to be jagged.

The micro-Raman spectra show the silicon optical phonon mode at 520 cm^{-1} generally weakens and is replaced by the disorder-induced broad response below 500 cm^{-1} that is indicative of amorphous silicon [8]. However, spectral lines are observed at 505 to 510 cm^{-1} in association with the 520 cm^{-1} line, when the focal plane of the Raman beam moves into the silicon and away from the silicon dioxide/silicon interface. Illustrative spectra are shown in Figure 1 for the as-implanted wafer with a dose of 2×10^{15} As/cm^2. The micro-Raman spectra of Figure 1 show the focal plane location of the incident laser beam plays a dominant role. The 0 curve has the focal plane at the sample surface and curves with the positive labels have focal planes within the silicon, but at a depth much less than the microscope stage curve label. As the focal plane enters the silicon, the amorphous silicon signal increases and a strong peak at 509 cm^{-1} appears. The latter decreases as the focal plane moves deeper into the silicon. The 515 cm^{-1} peak is probably a combination of the 509 and the 520 cm^{-1} lines. The incident laser power level is 2 mW for Figure 1. An increase of the incident power level enhances the 520 cm^{-1} line and a decrease weakens both lines. P/O Raman studies rule out silicon in the diamond phase as the source of the 505 to 510 cm^{-1} line and provide support for the Si-IV phase. In addition, the P/O work indicates the accompanying 520 cm^{-1} optical phonon line is not due to the substrate silicon. The as-implanted device wafer produces similar spectra, but the annealed device wafer shows only the 520 cm^{-1} line of crystalline silicon.

We interpret these experiments to mean there are well-localized crystallites just before the substrate crystalline silicon starts. The next two sections are a beginning toward an explanation of these experimental observations.

HEAT FLOW CALCULATIONS

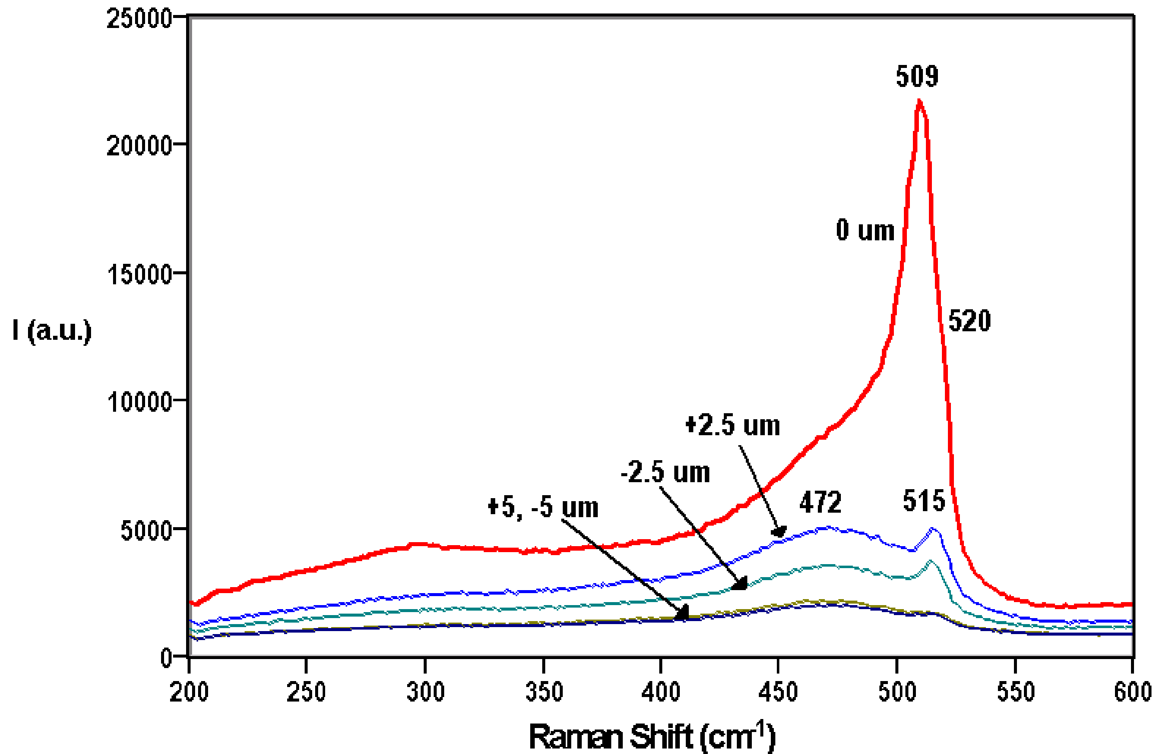

Figure 1. Micro-Raman spectra with the exciting laser at 514.5 nm and 2 mW. The curves are labelled with the microscope stage position and 0 indicates the focal plane is at the sample surface. The focal plane moves into the silicon when the curve labels are positive.

The spatial scale of a collision cascade is estimated with the Monte Carlo energy loss simulator TRIM [9]. The calculation indicates the depth of the damaged silicon is 0.1 to 0.15 µm and the lateral extent of a cascade is about 0.01 µm. The depth scale agrees with the TEM results alluded to in the previous section and with secondary ion mass spectroscopy profiles of the implanted arsenic. The TRIM results also hint that about 65 keV of the 150 keV per implanted arsenic ion goes into the silicon lattice. We estimate this takes the silicon atoms in the collision cascade above the 1681 K melting temperature of silicon. Molecular dynamics (MD) has been used [10] to simulate the response of the silicon lattice on the picosecond time scale and to estimate the temperature rise. For our present purposes, it suffices to build on the MD result that the silicon has melted locally. We also assume the entire melted region is at the same temperature.

A consideration of the scan pattern of a medium-current implanter [11], such as the ones that produced our samples, leads to a range of possibilities for the neighborhood of a collision cascade. The cascade can be surrounded by silicon that does not receive another implanted ion for a time on the order of milliseconds or more. This permits the liquid silicon volume to cool quickly. Intersecting solidification fronts may lead to defects in accordance with the MD results [10]. The other extreme is that many ions enter the silicon neighborhood within one scan and the resulting collision cascades overlap. This produces a large volume of liquid silicon, which justifies the following one-dimensional model.

The heat conduction equation is set up in one spatial dimension to follow the temperature within the silicon as a function of time. The model space starts with 0.1 µm of liquid silicon that runs from $z = 0.0$ to 0.1 µm. This is followed by 99.9 µm of crystalline silicon that is initially at

300 K. The silicon dioxide/silicon interface at z = 0 is assumed to be perfectly reflecting, while z = 100 µm is maintained at 300 K. The specific heat and thermal conductivity of crystalline silicon vary with temperature and are taken from Refs. 12 and 13, respectively. The parameters for liquid silicon are those used by Ref. 14. The melting temperature of silicon is assumed to be 1681 K and the heat of fusion is 39.6 kJ/mol [15]. Continuity of the temperature and the flux are assumed at the liquid silicon/crystalline silicon interface. At present, we assume the silicon has solidified when the heat of fusion has been removed.

An implicit scheme is used to solve the heat conduction equation. Illustrative results are shown in Figure 2 for an initial liquid silicon temperature of 1950 K. Four spatial points are tracked with time and the temperature plotted is the calculated temperature divided by 300 K. The liquid silicon cools quickly to the melting temperature and the heat of fusion is slowly removed over several microseconds. The time to solidify versus depth is plotted in Figure 3 for this case and for an initial temperature of 2850 K. It is apparent that the time to eliminate the heat of fusion dominates.

These calculations show that the damaged silicon undergoes a phase transformation and recrystallizes. The low dose arsenic implants show crystalline silicon [2,3] with a hint of amorphous silicon in the broadening of the 520 cm^{-1} line on the low-energy side. A model space with more spatial dimensions is needed to treat the isolated collision cascade case and to include the defect creation that the MD calculations find [10]. Higher doses require more effects as outlined in the next section.

HIGHER DOSES AND PHASE TRANSFORMATIONS

If one considers an element of the silicon surface that is about the lateral extent of a collision cascade, then one is led to an area 0.01 x 0.01 μm^2. For our lowest dose of 2 x 10^{13} As/cm^2, the

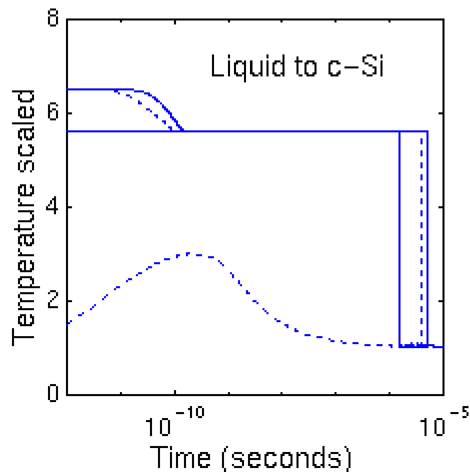

Figure 2. Calculated temperature divided by 300 K versus time for the spatial locations from top to bottom of 0.0, 0.05, 0.10, and 0.11 µm. Initially, liquid silicon = 1950 K.

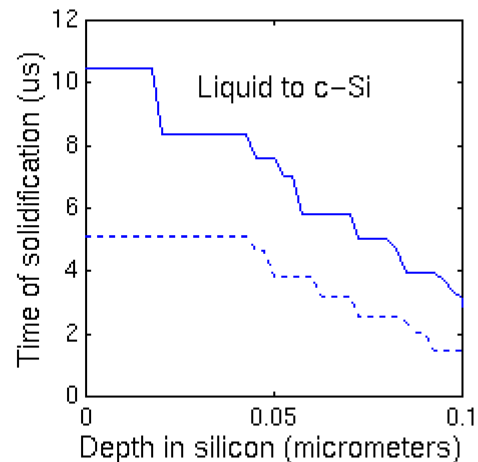

Figure 3. Time of solidification versus depth. Initial temperature: Solid curve = 2850 K, Dashed curve = 1950 K.

selected area receives an average of 20 arsenic atoms during the 1.4 s implant. Thus, we are tempted to suggest the silicon is melted and recrystallized numerous times while the implant is happening. It is likely that some defective regions develop during these events in accordance with the MD work [10]. Higher doses lead to more arsenic ions entering the selected area during an implantation time that scales at least linearly with dose. The highest dose of 5×10^{15} As/cm^2 puts an average of 5000 ions into the selected area. We suggest that defects continue to accumulate during these successive cascades. It is likely that crystalline silicon is eliminated from the local ion-implanted region. This would result in liquid silicon surrounded by silicon dioxide and defective silicon, which we assume to have the properties of amorphous silicon.

The time scale for solidification in this case is now investigated with our one-dimensional model. Liquid silicon occupies $z = 0$ to 0.1 µm. This is followed by 0.02 µm of amorphous silicon and 99.88 µm of crystalline silicon. The melting temperature is taken to be 1420 K [14] and the heat of fusion is assumed to be 30.5 kJ/mol. The latter is based on scaling the Ref. 14 value by the same factor needed to reduce the heat of fusion for crystalline silicon to the value we use in the previous section. The thermal conductivity for amorphous silicon is taken to be 1/150 that of crystalline silicon on the basis of Ref. 16. The results for the solidification of the liquid silicon into amorphous silicon appear in Figure 4 for an initial temperature of 1950 K. In comparison with Figure 2, the lower melting temperature means the liquid silicon takes longer to reach the melting temperature of 1420 K. The smaller heat of fusion for amorphous silicon permits a faster onset of continued temperature reduction. If the initial region of amorphous silicon is thicker, then the two time scales are lengthened. It appears the time scale for solidification into amorphous silicon is faster than the time scale for crystalline silicon formation when each is seeded appropriately.

Finally, we briefly consider the crystallites seen by the micro-Raman spectroscopy. A diamond phase crystallite may arise if some crystalline silicon is left to laterally seed the solidification and further cascades do not completely damage the crystallite. The lateral seed is suggested because the P/O Raman data indicate the 520cm^{-1} line is from Si-I, which is oriented differently than the crystalline silicon substrate.

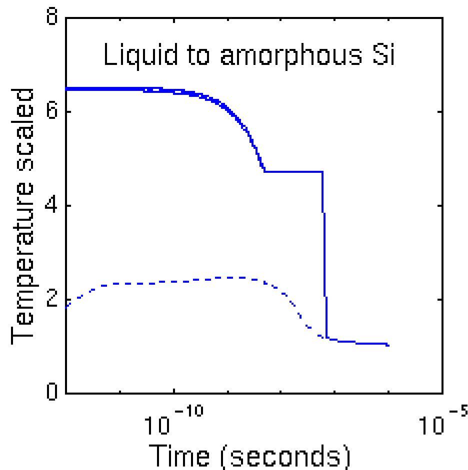

Figure 4. Calculated temperature divided by 300 K versus time for the spatial locations from top to bottom of 0.0, 0.05, 0.10, and 0.11 um. Initially, the liquid silicon = 1950 K

CONCLUSIONS AND EXTENSIONS

The present work builds on the picture of the energy loss from implanted arsenic ions turning a region of crystalline silicon into liquid silicon. The region cools and recrystallizes. This process repeats as new ions arrive in, and adjacent to, the region and may help explain some of the data on as-implanted silicon. While the model of the third section lacks the detailed treatment that molecular dynamics affords, it permits longer time scales to be treated. The present calculations are performed with one spatial dimension and they serve to explore the time scale for silicon solidification. The model needs to be extended into 2 or 3 spatial dimensions, so that defect creation and accumulation may be taken into account. It is clear that extensive work remains to establish the origins of the crystallites. The Si-IV crystallites are expected to require additional energy to form, because about 0.5 eV/atom [17] separates the hexagonal phase (Si-IV) from the Si-I diamond phase. Perhaps, several collision cascades within the liquid cooling period are needed to supply the additional energy to form Si-IV. It is more likely that the transformation described by Tan et al. [6] takes a Si-I crystallite into one of Si-IV with the needed energy coming from collision cascades. What happens when a new collision cascade disrupts a region of liquid silicon is also worthy of further study.

ACKNOWLEDGMENTS

We thank Jean Catone for the first series of arsenic implants and Hung Doan for the second series and the details of the ion implanters' scanning. JPL thanks Dr. Maria Caturla for discussions and copies of her dissertation and publications.

REFERENCES

1. J. P. Lavine and D. D. Tuschel, Bull.Am. Phys. Soc. **44**, 1338, paper SC08-8 (1999).
2. J. P. Lavine and D. D. Tuschel, MRS Symp. Proc. **588**, 149 (2000).
3. D. D. Tuschel and J. P. Lavine, MRS Symp. Proc. **588**, 227 (2000).
4. Y. Gogotsi, C. Baek, F. Kirscht, Semicond. Sci. Technol. **14**, 936 and 1019 (1999).
5. G. Weill, J. L. Mansot, G. Sagon, C. Carlone, J. M. Besson, Semicond. Sci. Technol. **4**, 280 (1989).
6. T. Y. Tan, H. Foll, S. M. Hu, Philos. Mag. **A44**, 127 (1981).
7. H. Cerva, J. Mater. Res. **6**, 2324 (1991).
8. J. S. Lannin, Semiconduct. and Semimet. **21**, Part B, Ch. 6 (1984).
9. J. F. Ziegler, J. P. Biersack, U. Littmark, *The Stopping and Range of Ions in Solids* (Pergamon Press, New York, 1985).
10. M. -J. Caturla, T. Diaz de la Rubia, L. A. Marques, G. H. Gilmer, Phys. Rev. **B54**, 16683 (1996).
11. H. Glawischnig, J. O'Connor, F. Sinclair, M. Harris, M. Current, in *Ion Implantation Science and Technology*, edited by J. Ziegler (Ion Implantation Technology Co., Yorktown, NY, 1996) Ch. 7.
12. H. -M. Kagaya and T. Soma, in *Properties of Silicon*, EMIS Datareviews Series No. 4 , Section 1.13 (1988).
13. M. N. Wybourne, in *Properties of Silicon*, *ibid.*, Section 1.14 (1988).
14. M. Toulemonde, C. Dufour, E. Paumier, Phys. Rev. **B46**, 14362 (1992).
15. M. de Podesta, *Understanding the Properties of Matter* (UCL Press, London, 1996) p 329.
16. Y. S. Ju and K. E. Goodson, *Microscale Heat Conduction in Integrated Circuits and Their Constituent Films* (Kluwer Academic, Boston, 1999) Ch. 4.
17. R. J. Needs and A. Mujica, Phys. Rev. **B51**, 9652 (1995).